

# Production of $\eta'$ Mesons in the $pp \rightarrow pp\eta'$ Reaction at 3.67 GeV/c

F. Balestra<sup>d</sup> Y. Bedfer<sup>c</sup> R. Bertini<sup>c,d</sup> L.C. Bland<sup>b</sup>  
 A. Brenschede<sup>h,1</sup> F. Brochard<sup>c,2</sup> M.P. Bussa<sup>d</sup>  
 Seonho Choi<sup>b,3</sup> M. Debowski<sup>f,4</sup> M. Dzemiđic<sup>b,5</sup>  
 J.-Cl. Faivre<sup>c</sup> I.V. Falomkin<sup>a,6</sup> L. Fava<sup>e</sup> L. Ferrero<sup>d</sup>  
 J. Foryciarz<sup>g,f,7</sup> I. Fröhlich<sup>h</sup> V. Frolov<sup>a</sup> R. Garfagnini<sup>d</sup>  
 A. Grasso<sup>d</sup> S. Heinz<sup>c</sup> V.V. Ivanov<sup>a</sup> W.W. Jacobs<sup>b</sup> W. Kühn<sup>h</sup>  
 A. Maggiora<sup>d</sup> M. Maggiora<sup>d</sup> A. Manara<sup>c,d</sup> D. Panzieri<sup>e</sup>  
 H.-W. Pfaff<sup>h</sup> G. Piragino<sup>d</sup> G.B. Pontecorvo<sup>a</sup> A. Popov<sup>a</sup>  
 J. Ritman<sup>h</sup> P. Salabura<sup>f</sup> V. Tchalyshev<sup>a</sup> F. Tosello<sup>d</sup>  
 S.E. Vigdor<sup>b</sup> G. Zosi<sup>d</sup>

<sup>a</sup>*JINR, Dubna, Russia*

<sup>b</sup>*Indiana University Cyclotron Facility, Bloomington, Indiana, U.S.A.*

<sup>c</sup>*Laboratoire National Saturne, CEA Saclay, France*

<sup>d</sup>*Dipartimento di Fisica "A. Avogadro" and INFN - Torino, Italy*

<sup>e</sup>*Universita' del Piemonte Orientale and INFN - Torino, Italy*

<sup>f</sup>*M. Smoluchowski Institute of Physics, Jagellonian University, Kraków, Poland*

<sup>g</sup>*H.Niewodniczanski Institute of Nuclear Physics, Kraków, Poland*

<sup>h</sup>*II. Physikalisches Institut, University of Gießen, Germany*

<sup>i</sup>*TRIUMF - Vancouver, Canada*

DISTO Collaboration

---

## Abstract

The ratio of the total exclusive production cross sections for  $\eta'$  and  $\eta$  mesons has been measured in the  $pp$  reaction at  $p_{beam} = 3.67$  GeV/c. The observed  $\eta'/\eta$  ratio is  $(0.83 \pm 0.11_{-0.18}^{+0.23}) \times 10^{-2}$  from which the exclusive  $\eta'$  meson production cross section is determined to be  $(1.12 \pm 0.15_{-0.31}^{+0.42}) \mu b$ . Differential cross section distributions have been measured. Their shape is consistent with isotropic  $\eta'$  meson production.

*Key words:*  $\eta'$  meson, proton-proton final state interaction

*PACS:* 14.40.Cs, 13.75.Cs, 25.40.Ve

---

The study of the  $\eta'$  meson production is of particular interest because of its large mass compared to the other members of the ground state pseudoscalar meson nonet. The spontaneous breaking of chiral symmetry causes the existence of massless Goldstone bosons, which acquire mass due to explicit chiral symmetry breaking, and are associated with the pseudoscalar meson nonet. In addition quantization effects in QCD lead to the so-called  $U_A(1)$  anomaly, which allows the  $\eta'$  meson to gain mass by a different mechanism than the Goldstone bosons [1–5]. Nevertheless, the origin of the  $\eta'$  mass and its structure in terms of quark and gluon degrees of freedom remain controversial.

Recent measurements of the  $\eta'$  meson by the CLEO collaboration show an anomalously large branching ratio of B-mesons to  $\eta'X$  and  $\eta'K$  [6], which might indicate a strong coupling of the  $\eta'$  meson to gluons [7]. Furthermore, the quark component of the nucleon's axial-vector matrix element measured in the EMC experiment [8] suggests that the  $\eta'$  meson couples very weakly to the nucleon [9,10].

First measurements [11–13] of the reaction  $pp \rightarrow pp\eta'$  near the production threshold provide the possibility to determine the coupling constant  $g_{\eta'NN}$ . However, a quantitative evaluation of this coupling constant requires answers to several open questions concerning the production mechanism, such as the roles of (i) meson-exchange currents, (ii) baryon resonances in the production mechanism (comparable with the role of the  $N^*(1535)$  for  $\eta$  meson production [14]), and (iii) final-state interactions (FSI).

The existing data close to threshold are consistent with different one-boson-exchange models (OBE) including FSI [15,16] given the ambiguities in the treatment of heavy-meson-exchange currents. Evaluation of the different models requires a consistent description over a wide energy range, but data have been lacking at higher energies, where identification of the  $\eta'$  production can no longer be made solely by detecting two protons in a small forward cone [11–13].

In this letter, we report on a measurement of the  $\eta'/\eta$  production cross section ratio at an energy where proton-proton ( $pp$ ) FSI have a much smaller

---

<sup>1</sup> current address: Brokat Infosystems AG - Stuttgart

<sup>2</sup> current address: LPNHE X, Ecole Polytechnique Palaiseau

<sup>3</sup> current address: Temple University, Philadelphia

<sup>4</sup> current address: FZ-Rossendorf

<sup>5</sup> current address: IU School of Medicine - Indianapolis

<sup>6</sup> deceased

<sup>7</sup> current address: Motorola Polska Software Center - Kraków

relative influence on the production mechanism [16,17] compared to the near to threshold data [11–13]. In addition, we show the differential cross sections of the  $\eta'$  meson as a function of the polar angle in the CM (center of mass) reference frame and the momentum distributions of the final state particles. These distributions are related to the partial wave contribution in the exit channel ( $pp\eta'$ ).

We studied the  $pp$  reaction at the SATURNE II accelerator facility at Saclay. The proton beam of momentum 3.67 GeV/c was incident on a liquid hydrogen target and charged products were detected using the DISTO spectrometer, which is described in detail elsewhere [18]. This spectrometer consisted of a large dipole magnet (40 cm gap size, operating at 1.0 Tm) which covered the target area and two sets of scintillating fiber hodoscopes. Outside the magnetic field, two sets of multi-wire proportional chambers (MWPC) were mounted, along with segmented plastic scintillator hodoscopes and water Čerenkov detectors. The scintillator hodoscopes and the Čerenkov detectors allow particle identification by combining either the energy loss, time of flight or Čerenkov light output with the particle momentum.

The large acceptance of all detectors ( $\simeq 2^\circ$  to  $\simeq 48^\circ$  horizontally and  $\simeq \pm 15^\circ$  vertically), on both sides of the beam, facilitated the coincident measurement of four charged particles, which was crucial for the reconstruction of many exclusive channels like  $ppK^+K^-$  [19,20],  $pp\pi^+\pi^-\pi^0$ ,  $pK\Lambda$  and  $pK\Sigma$  [21].

The multi-particle trigger [22], which was based on the multiplicity of the hodoscope elements and the scintillating fibers, selected events with at least three charged tracks in the final state. The results presented in this work are based on  $4.2 \times 10^7$  reconstructed events with four charged particles (mainly  $pp\pi^+\pi^-$ ) detected.

The exclusive  $\eta$  meson production ( $pp \rightarrow pp\eta$ ) was identified via its dominant decay channel involving charged particles ( $\pi^+\pi^-\pi^0$ , branching ratio 23.1%) and the reaction  $pp \rightarrow pp\eta'$  was reconstructed via the decay of the  $\eta'$  meson into  $\pi^+\pi^-\eta$  (branching ratio 43.8%). The selection of the exclusive  $\eta'$  and  $\eta$  meson production is based on two kinematical observables, the 4-particle ( $pp\pi^+\pi^-$ ) missing mass ( $M_{miss}^{4p}$ ) and the proton-proton missing mass ( $M_{miss}^{pp}$ ). Furthermore the light output from the Čerenkov detectors together with the particle momentum were used to discriminate between  $\pi^+$  mesons and protons in the final state.

Since neutral pions were not detected ( $\pi^0 \rightarrow \gamma\gamma$ , branching ratio 98.8%),  $pp\eta$  events were selected in which  $M_{miss}^{4p}$  was approximately consistent with a missing  $\pi^0$  meson ( $0.005 \text{ GeV}^2/c^4 < (M_{miss}^{4p})^2 < 0.035 \text{ GeV}^2/c^4$ ). After imposing this constraint the proton-proton missing mass distribution is shown in Fig. 1 (upper frame). A broad signal from the  $\eta$  meson is visible near

$$M_{miss}^{4p} \simeq 0.3 \text{ GeV}^2/c^4.$$

The assumption of a missing  $\pi^0$  meson allowed a constraint  $((M_{miss}^{4p})^2 = M_{\pi^0}^2)$  to be imposed in order to improve the  $(M_{miss}^{pp})^2$  mass resolution by a kinematical refit procedure. In this procedure all particle momenta were simultaneous re-determined under the assumption of a missing  $\pi^0$  meson. After applying the refit procedure, the resolution of the  $\eta$  meson signal in the  $(M_{miss}^{pp})^2$  distribution is improved by about a factor 2 (see Fig. 1, lower frame).

In both frames the solid curve shows the sum of the signal (dotted curve) and the background (dashed curve). The signal line shape was taken from detailed Monte Carlo simulations of the detector performance and the yield was determined by scaling the line shape to match the data using a  $\chi^2$  minimization procedure. The small deviations at  $(M_{miss}^{pp})^2 \simeq 0.325 \text{ GeV}^2/c^4$  result from imperfections of the modeling of the detector response and are included in the estimation of the systematic errors.

The non-resonant reaction  $pp \rightarrow pp\pi^+\pi^-\pi^0$  accounts for most of the background under the  $\eta$  meson signal. Since the exact shape of the background is not quantitatively known, the background has been parameterized with a 3<sup>rd</sup> order polynomial, that provides the best  $\chi^2$  to the fit.

The reconstruction of the decay channel  $pp \rightarrow pp\eta' \rightarrow pp\pi^+\pi^-\eta$  is analogous to the  $\eta$  meson reconstruction described above, since the  $\eta$  meson decays mostly by neutral modes (branching ratio 71.5%).

For this decay channel  $M_{miss}^{pp}$  and  $M_{miss}^{4p}$  must correspond to a missing  $\eta'$  and a missing  $\eta$ , respectively. The  $(M_{miss}^{pp})^2$  distribution for events with a 4-particle missing mass consistent with a missing  $\eta$  meson (i.e.  $|(M_{miss}^{4p})^2 - M_{\eta}^2| < 0.03 \text{ GeV}^2/c^4$ ) is shown in Fig. 2 before (hatched area) and after (data points) the kinematical refit procedure with the constraint  $M_{miss}^{4p} = M_{\eta}$ . The spectrum after the refit shows a clear signal from the  $\eta'$  meson near  $M_{\eta'}^2 \simeq 0.92 \text{ GeV}^2/c^4$ . In comparison to the reconstruction of the  $\eta$  meson the kinematical refit procedure only improves the resolution of the  $\eta'$  signal by about 25%, due to the lower laboratory momenta of the outgoing protons.

The dashed curve represents the background contribution and the solid curve shows the sum of the background and the signal (dotted curve). The shape of the signal was determined from the Monte Carlo simulations and the yield was determined analogously as described above for the  $\eta$  meson yield. The background below the  $\eta'$  meson signal originates mainly from non-resonant  $pp \rightarrow pp\eta\pi^+\pi^-$  production and reactions such as  $pp \rightarrow pp\pi^+\pi^-\pi\pi$  where two pions are not detected. Since the exact form is unknown, the shape of the background was parameterized as a 4<sup>th</sup> order polynomial, that provides the best  $\chi^2$  to the fit.

The relative acceptance correction of the DISTO spectrometer for the  $pp\eta'$  vs.  $pp\eta$  channels has been determined using Monte Carlo simulations which were analyzed as the measured data.

The detector acceptance was determined as a 4-dimensional function of all relevant degrees of freedom in the  $pp\eta'$  and  $pp\eta$  final states.

The five degrees of freedom related to the three body decay of the  $\eta'$  and the  $\eta$  mesons were integrated in the simulations using an isotropic orientation of the decay plane and the measured matrix elements [23,24].

After accounting for azimuthal symmetry in the production reaction, we divided the kinematically allowed phase space into four-dimensional bins and evaluated the efficiency for each bin separately. This was realized by storing the number of generated and the number of reconstructed events from the simulations for each phase space bin. The bin-by-bin ratio provides the efficiency correction, which was stored in the 4-dimensional acceptance correction matrix.

The acceptance values were typically larger than 1 % in each phase space bin including branching ratios, particle decay in flight, tracking efficiency and particle identification efficiency. The approximately 6 % efficiency loss due to the refit procedure was also accounted for. The data were corrected using the appropriate entry from this 4-dimensional acceptance correction matrix, on an event by event basis. For a detailed discussion of the relative acceptance correction method see [25].

The simulations indicated a very low acceptance of the apparatus for  $\eta$  mesons produced in the backward hemisphere in the CM (center of mass) rest frame. However, since the entrance consists of two identical particles a reflection symmetry about  $\Theta_{CM} = 90^\circ$  exists, thus the backward data are redundant for determining total cross sections. Therefore, we only analyzed the acceptance-corrected production yield in the forward hemisphere, where the acceptance was non-zero in each phase space bin.

It should be noted that the acceptance correction is essentially independent of the event generator used in the simulations due to the complete phase space coverage of the DISTO spectrometer. The generator used for the correction assumed uniform phase space density for both reactions. This assumption was verified by using the same correction for different phase space populations in the simulations. The small deviations observed are included in the estimation of the systematic errors.

Furthermore, the simulations included all important decay modes for the  $\eta$  meson [26] for the acceptance correction of the  $pp \rightarrow pp\eta' \rightarrow pp\pi^+\pi^-\eta$  and the  $pp \rightarrow pp\eta$  reactions. Hence, background processes such as  $\eta' \rightarrow \pi^+\pi^-\eta \rightarrow$

$\pi^+\pi^-(\pi^+\pi^-\pi^0)$ , where one or both of the observed pions are from the  $\eta$  or events with more than four charged particles in the acceptance of the detector are properly accounted for.

After correcting the  $\eta'$  meson and the  $\eta$  meson production yields for the respective acceptances and branching ratios [26] as described above, the measured total cross section ratio  $R = \sigma_{pp \rightarrow pp\eta'}/\sigma_{pp \rightarrow pp\eta}$  is determined to be  $(0.83 \pm 0.11^{+0.23}_{-0.18}) \times 10^{-2}$ . Where the first error is statistical and the second error range is due to systematic uncertainties. Because both meson channels have been reconstructed in events with the same four-charged-particle final state and measured simultaneously within the same experiment, many systematic uncertainties cancel when considering the production ratio. As a result, the systematic error is dominated by the background subtraction and the relative acceptance correction.

The total cross section for the  $pp \rightarrow pp\eta$  reaction is known over a wide energy range [27] above and below the beam momentum of this measurement. Interpolation of the existing data leads to a cross section of  $\sigma_{pp \rightarrow pp\eta}^{exp} = 135 \pm 35 \mu b$  at  $p_{beam} = 3.67$  GeV/c in good agreement of the value  $\sigma_{pp \rightarrow pp\eta}^{model} \simeq 120 \mu b$  calculated by Vetter et al. [14] using a meson exchange model. By multiplying  $R$  by  $\sigma_{pp \rightarrow pp\eta}^{exp}$  we obtain the total cross section  $\sigma_{pp \rightarrow pp\eta'} = 1.12 \pm 0.15^{+0.42}_{-0.31} \mu b$ . The systematic error in  $\sigma_{pp \rightarrow pp\eta}^{exp}$  is geometrically added with the systematic error in the  $pp \rightarrow pp\eta'/pp \rightarrow pp\eta$  ratio. This result is shown in Fig. 3 (filled circle) together with other data closer to the production threshold [11–13] and model calculations (solid and dashed curves) [16].

The calculation from Sibirtsev et al. [16] represents a one-pion-exchange model including the  $pp$  FSI. The solid line denotes the full calculation and the dashed line corresponds to the same calculation excluding the FSI. The full calculation reproduces the near threshold data well, but predicts a cross section of about  $2.3 \mu b$  at our energy, which is significantly above our measurement.

The distribution of the differential cross section as a function of the CM polar angle of the  $\eta'$  meson ( $\cos(\Theta_{CM})$ ) is shown in Fig. 4. The distribution displays no significant deviations from isotropy, indicating that the  $\eta'$  meson is predominantly in a s-wave state relative to the two protons. The differential cross section distributions were determined by producing the corresponding  $(M_{miss}^{pp})^2$  spectra for each kinematical bin. Each spectrum was fitted analogously as described above to determine the yield of the signal for each bin. The statistical uncertainty of the yield for each bin are determined by the fitting procedure and are shown as vertical error bars in the differential distributions (see Fig. 4 and Fig. 5). The signal line shape was calculated for each spectrum individually from the Monte Carlo simulations and the background was also allowed to vary.

The relative partial wave contributions in the three particle final state  $pp\eta'$  can also be determined from the momentum distributions  $q$  and  $p$ , where  $q$  is the CM momentum of the  $\eta'$  meson and  $p$  is the momentum of a proton in the proton-proton rest frame.

Then, the total cross section is given as the sum of the individual partial wave contributions [28]:

$$\sigma \sim \sum_{l_1, l_2} \int |M_{l_1, l_2}|^2 d\rho_{l_1 l_2}. \quad (1)$$

here the sum extends over the angular momenta  $l_1, l_2$  and the transition amplitude for the given exit channel ( $M_{l_1, l_2}$ ), where  $l_1$  is the orbital angular momentum of the two protons relative to each other and  $l_2$  is the orbital angular momentum of the  $\eta'$  meson relative to the proton-proton system.

The corresponding phase space element  $d\rho_{l_1 l_2}$  is determined by

$$d\rho_{l_1 l_2} \sim p^{2l_1+1} q^{2l_2+2} dq, \quad (2)$$

If we assume the transition amplitude  $M_{l_1, l_2}$  to be almost constant over the available phase space then the differential cross section as a function of the particle momenta are given by the variation of the phase space volume.

The measured differential cross sections are plotted in Fig. 5. as a function of  $q$  (upper frame) and  $p$  (lower frame). The corresponding curves, that reproduce the data quite well, have been obtained from equation 2, assuming  $l_1 = l_2 = 0$ . The normalization was obtained by a simultaneous  $\chi^2$  minimization to both differential cross section distributions. The introduction of higher values of  $l$  does not improve the  $\chi^2$  fit to the data. The result is consistent with a dominant Ss-wave production of the  $\eta'$  meson, where S denotes  $l_1 = 0$  and s  $l_2 = 0$ , respectively.

In conclusion, the production of the pseudoscalar  $\eta'$  meson has been studied in the  $pp$  reaction at  $p_{beam} = 3.67$  GeV/c. The  $\eta'$  meson has been reconstructed by measuring its charged decay products. The  $\eta'/\eta$  cross section ratio has been determined and the extracted  $\eta'$  cross section has been compared to data very close to threshold and an one-pion exchange model including the  $pp$  FSI. While the model describes the data close to threshold very well it overestimates our data point by about 100 %.

Furthermore, the differential cross sections indicates that the  $\eta'$  meson is predominantly produced in a s-wave state for the two protons relative to each other and the  $\eta'$  meson relative to the proton-proton system.

Calculations up to 100 MeV above the  $\eta'$  production threshold, in the framework of a relativistic meson-exchange model [29] should be extended to higher energies. Comparison with our results should help to learn more about the different  $\eta'$  meson production mechanisms, the potential influence of a  $\eta'/p$  FSI [30] and the magnitude of the coupling constant  $g_{\eta'pp}$ .

In this context a comparison with a recent publication on the production of  $\pi^0$ ,  $\eta$  and  $\eta'$  mesons in proton-proton collisions [31] should be very helpful. The novel approach therein factored out the  $pp$  FSI and the initial-state proton-proton interaction (ISI) from the total cross section to determine the phase space dependence of the total production amplitude for  $\pi^0$  ( $|A_0^\pi|$ ),  $\eta$  ( $|A_0^\eta|$ ) and  $\eta'$  mesons ( $|A_0^{\eta'}|$ ).

Our measurement will assist to evaluate different models used for the parameterization of the  $pp$  FSI which is essential for the determination of the absolute strength of  $|A_0^{\eta'}|^2$  and hence of  $g_{\eta'pp}$ .

This paper is dedicated to the memory of Igor Falomkin.

We acknowledge the work provided by the SATURNE II accelerator staff and technical support groups in delivering an excellent proton beam and assisting this experimental program.

This work has been supported in part by: CNRS-IN2P3, CEA-DSM, NSF, INFN, KBN (2 P03B 117 10 and 2 P03B 115 15) and GSI.

## References

- [1] S. Weinberg, Phys. Rev. D 11 (1975) 3583.
- [2] E. Witten, Nucl. Phys. B 156 (1979) 269.
- [3] G. Veneziano, Nucl. Phys. B 159 (1979) 213.
- [4] G. 't'Hooft, Phys. Rev. Lett. 37 (1976) 8; G. 't'Hooft, Phys. Rev. D 14 (1976) 3432.
- [5] A.De Rejula, H. Georgi and S.L. Glashow, Phys.Rev. D 12 (1975) 147.
- [6] B.H. Behrens et al., Phys. Rev. Lett. 80 (1998) 3710; T.E. Browder et al., Phys. Rev. Lett. 81 (1998) 1786.
- [7] D. Atwood and A. Somi, Phys. Rev. Lett. 79 (1997) 5206.
- [8] J. Ashman et al., Phys. Lett. B 206 (1988) 364.
- [9] T. Hatsuda, Nucl. Phys. B 329 (1990) 376.



- [10] G.M. Shore and G. Veneziano, Phys. Lett. B 244 (1990) 75.
- [11] P. Moskal et al. Phys. Rev. Lett 80 (1998) 3202.
- [12] F. Hibou et al. Phys. Lett. B 438 (1998) 41.
- [13] P. Moskal et al. Phys. Lett. B 474 (2000) 416.
- [14] T. Vetter et al., Phys. Lett. B 263 (1991) 153.
- [15] V. Bernard, N. Kaiser and U.-G. Meißner, Eur. Phys. J. A 4 (1999) 259.
- [16] A. Sibirtsev and W. Cassing, Eur. Phys. J. A 2 (1998) 333.
- [17] G. Fäldt and C. Wilkin, Z. Phys. A 357 (1997) 241.
- [18] F. Balestra et al., Nucl. Instr. Meth. A 426 (1999) 385.
- [19] F. Balestra et al., Phys. Rev. Lett. 81 (1998) 4572.
- [20] F. Balestra et al., Phys. Lett. B468 (1999) 385.
- [21] F. Balestra et al., Phys. Rev. Lett. 83 (1999) 1534.
- [22] F. Balestra et al., IEEE Trans. Nucl. SCI. 45 (1998) 817.
- [23] G.R. Kalbfleisch, Phys. Rev. 10 (1974) 916.
- [24] C. Amsler et al., Phys. Lett. B 346 (1995) 203.
- [25] F. Balestra et al., submitted to Phys. Rev. C.
- [26] C. Caso et al., Eur. Phys. J. C 3 (1998) 1.
- [27] J. Smyrski et al., Phys. Lett. B 474 (2000) 182; H. Calán et al., Phys. Lett. B 366 (1996) 39; A. M. Bergdolt et al., Phys. Rev. D 48 (1993) R2969; E. Chiavassa et al., Phys. Lett. B 322 (1994), 270 (1994); E. Pickup et al, Phys. Rev. Lett. 8 (1962) 329; L. Bodini et al., Nuov. Cim. 58 A (1968) 475; A. P. Colleraine and U. Nauenberg, Phys. Rev. 161 (1967) 1387; G. Alexander et al., Phys. Rev. 154 (1967) 1284; C. Caso et al., Nuov Cim. 55 A (1968) 66; E. Colton and E. Gellert, Phys. Rev. D 1 (1970) 1979; G. Yekutie et al., Nucl. Phys. B 18 (1970) 301; S.P. Almeida et al., Phys. Rev. 174 (1968) 1638; J. Le Guyader et al., Nucl. Phys. B 35 (1971) 573.
- [28] R.G. Newton, Scattering Theory of Waves and Particles, Springer Verlag, New York. H.O. Meyer, Particles and Fields Series 41, AIP Conference Proceedings, New York.
- [29] K. Nakayama et al., Phys. Rev. C 61 (2000) 024001.
- [30] V. Baru et al., Eur. Phys. J. A 6 (1999) 445.
- [31] P. Moskal et al. Phys. Lett. B 482 (2000) 356.

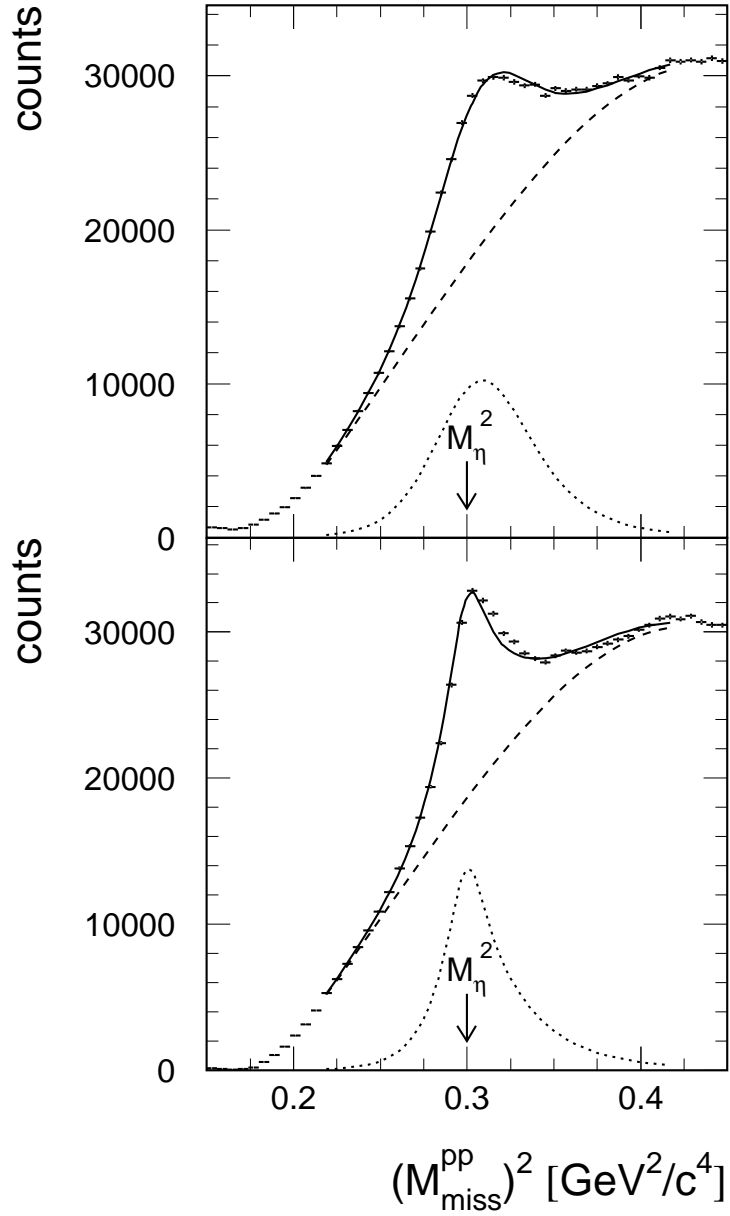


Fig. 1. Raw spectrum of  $(M_{miss}^{pp})^2$  for events with four charged particles ( $pp\pi^+\pi^-$ ) in the final state and a 4-particle missing mass ( $M_{miss}^{4p}$ ) consistent with a missing  $\pi^0$  meson. Before (upper frame) and after (lower frame) a kinematical refit procedure was applied to the data. The dashed curve represents the background contribution and the solid curve shows the sum of the background and of the signal (dotted curve).

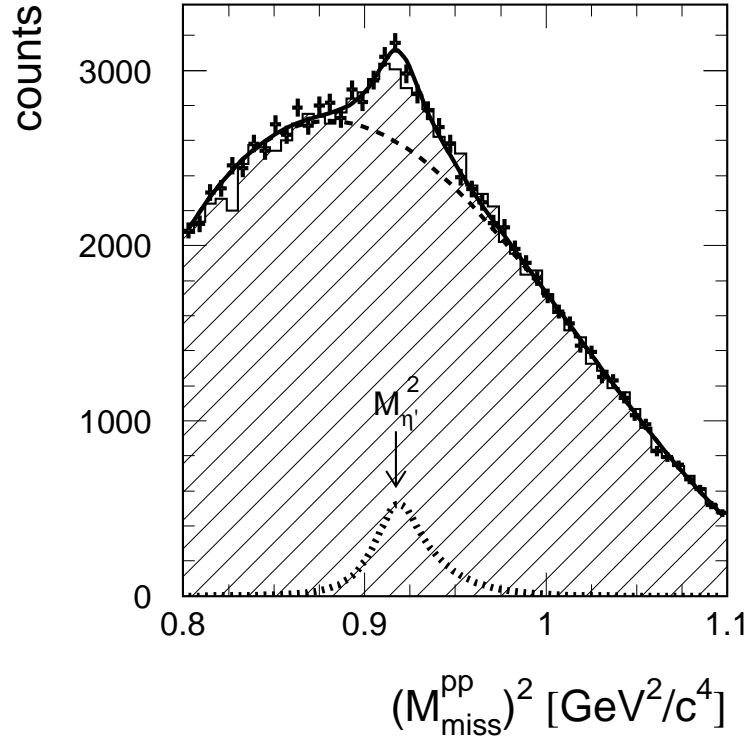


Fig. 2. Raw spectrum of  $(M_{\text{miss}}^{\text{pp}})^2$  for events with four charged particles ( $pp\pi^+\pi^-$ ) in the final state and a 4-particle missing mass ( $M_{\text{miss}}^{4p}$ ) consistent with a missing  $\eta$  meson. The data points show the spectrum after a kinematical refit procedure was applied. The dashed curve represents the background contribution and the solid curve shows the sum of the background and of the signal (dotted curve). In addition the hatched spectrum indicates the spectrum before the refit procedure was applied.

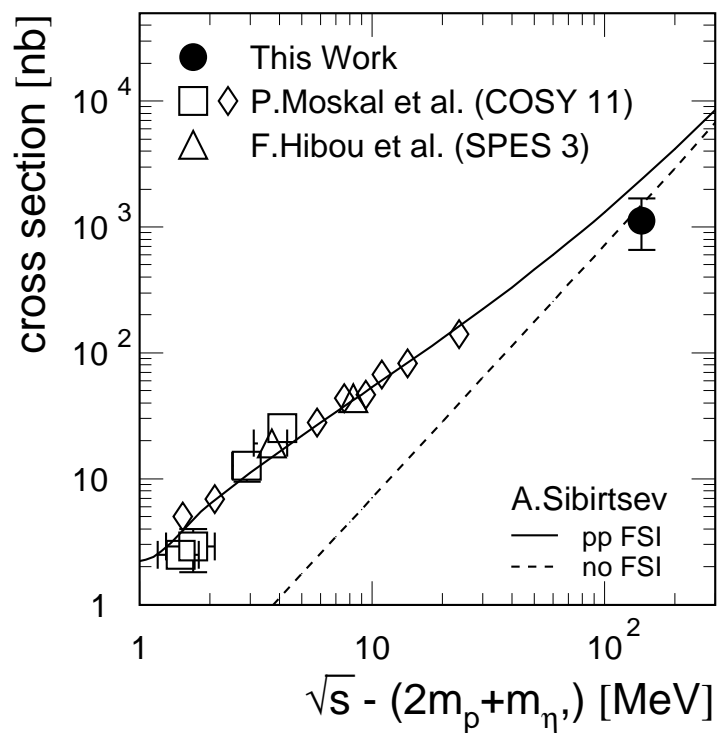


Fig. 3. Total cross section for the  $pp \rightarrow pp\eta'$  reaction as a function of the available energy above the  $\eta'$  production threshold. Shown is the value measured in this work (full circle) together with other data and model calculations described in the text.

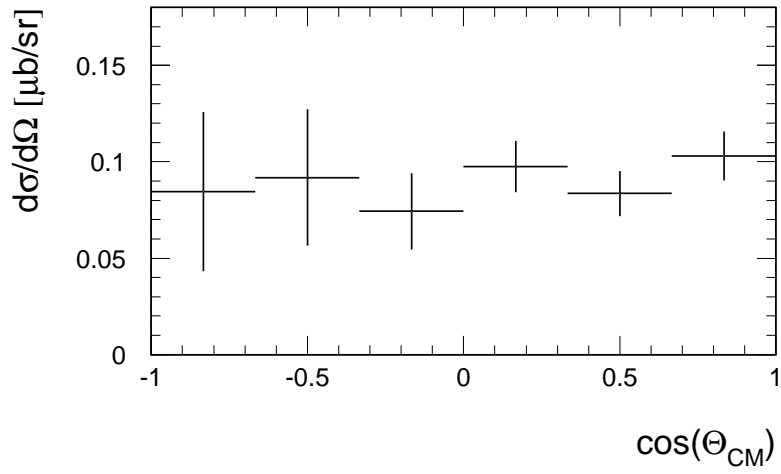


Fig. 4. Differential cross section for the  $pp \rightarrow pp\eta'$  reaction as a function of the CM polar angle of the  $\eta'$  meson

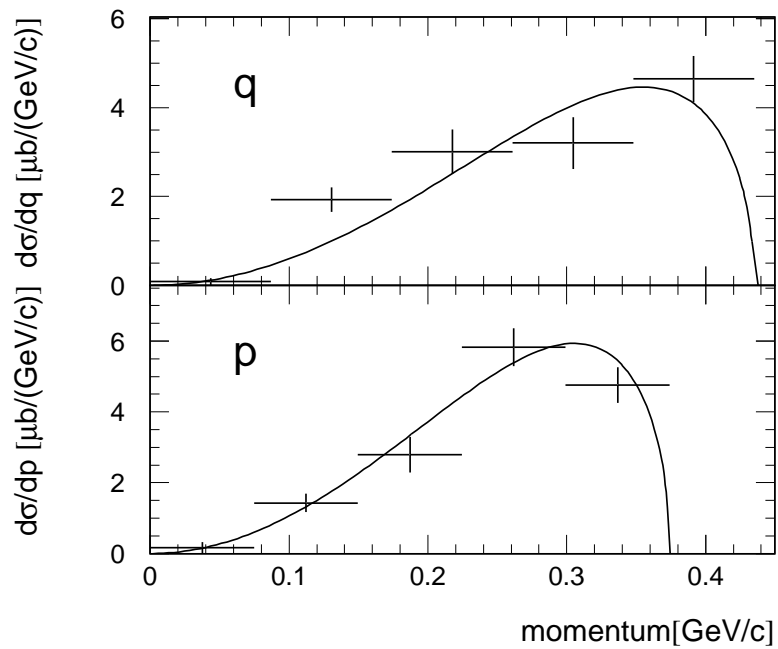


Fig. 5. Differential cross section for the  $pp \rightarrow pp\eta'$  reaction as a function of the  $\eta'$  meson momentum in the CM frame ( $q$ , upper frame) and the proton momentum in the  $pp$ -rest frame ( $p$ , lower frame). The curves denote the behavior of the three body phase space when the two protons are in a relative s-wave state and the  $\eta'$  meson is in a s-wave state relative to the protons.